Lab on a Chip

Viscosity-aided electromechanical poration of cells for transfecting molecules

Journal:	*Lab on a Chip*
Manuscript ID	LC-ART-07-2022-000628.R1
Article Type:	Paper
Date Submitted by the Author:	26-Aug-2022
Complete List of Authors:	Huang, Wenjing; Kyushu University, Department of Mechanical Engineering Sakuma, Shinya; Kyushu University, Department of Mechanical Engineering Tottori, Naotomo; Kyushu University, Department of Mechanical Engineering Sugano, Shigeo S.; National Institute of Advanced Industrial Science and Technology Tsukuba Center Tsukuba Central, Bioproduction Research Institute Yamanishi, Yoko; Kyushu University, Mechanical Engineering

Lab on a Chip

ARTICLE

Viscosity-aided electromechanical poration of cells for transfecting molecules

Received 00th January 20xx,
Accepted 00th January 20xx

DOI: 10.1039/x0xx00000x

Wenjing Huang, [a] Shinya Sakuma, [a] Naotomo Tottori, [a] Shigeo S. Sugano *[b] and Yoko Yamanishi *[a]

Cell poration technologies offer opportunities not only to understand the activities of biological molecules but also to investigate genetic manipulation possibilities. Unfortunately, transferring large molecules that can carry huge genomic information is challenging. Here, we demonstrate electromechanical poration using a core-shell-structured microbubble generator, consisting of a fine microelectrode covered with dielectric material. By introducing a microcavity at its tip, we could concentrate electrical field with the application of electric pulses and generate microbubbles for electromechanical stimulation of cells. Specifically, the technology enables transfection with molecules that are thousands of kDa even into osteoblasts and *Chlamydomonas*, which are generally considered to be difficult to inject. Notably, we found that the transfection efficiency can be enhanced by adjusting the viscosity of the cell suspension, which was presumably achieved by remodeling of the membrane cytoskeleton. The applicability of the approach to a variety of cell types opens up numerous emerging gene engineering applications.

Introduction

Cell poration technologies—methods of perforating cell membranes—offer opportunities not only to understand the functions of biological molecules [1-3] but also to investigate genetic manipulation [4-7]. Electroporation technologies enable transcellular delivery of biological/artificial materials such as proteins, nucleic acids, their vectors, and sensor particles, for genetic modulation and intercellular sensing [8-12]. Additionally, artificially mass-produced synthetic antibodies, enzymes, and cloned vectors have become available by utilizing live cell functions of the introduced materials [13]. For example, Bouvette et al. developed a method to purify 4–9 mg of human Dicer in a single day by transfection of human HEK293-EBNA1 cells with a pTT5 expression vector carrying a CMV promoter and the Epstein-Barr virus origin of replication oriP [13]. These delivered materials were categorized into several types by Stewart et al.; small drugs, molecular probes, cryoprotectants, proteins and peptides, nucleic acids, and synthetic nanomaterials and devices [14]. Among these materials, large molecules have recently attracted significant attention owing to their capacity for high-volume genomic information to replicate complex proteins. By combining with the CRISPR-Cas system—one of the most powerful tools for gene editing—the arbitrary target region of the genome inside the cell can be manipulated, with the components generally encoding large extra-chromosomal expression vectors (>10 kbp) by Cas endonucleases [15, 16]. Thus, transfecting with large molecules accelerates gene manipulation, and leads to biological discoveries and their application.

One of the critical concerns in cell poration is which method to use for transferring molecules into cells. We therefore focus on the physical methods that utilize field energies such as electroporation using electrical fields and sonoporation using pressure fields [17, 18]. In these methods, it is thought that cell membranes are perforated by the physical energy and molecules are transferred into the cell by diffusion, electrophoresis, and pressure transportation like injection through the perforated holes [19-21]. While viral or chemical methods of transfection have limited drug carrying capacity owing to the limited size of the viral capsid, toxicity, and cell-type dependent uptake [22-24]; physical methods intrinsically enable transfection with large molecules [25-29]. Although physical methods enable transfection with molecules without chemical/biological side effects, there are challenges related to transferring large molecules carrying huge genetic information. Among the physical methods, electroporation is widely adopted in various fields owing to its applicability to a variety of cell types and culture conditions [9]. When electrical pulses are applied to a cell suspension, the trans-membrane voltage of the single cells increases, which attracts positive ions from the surrounding environment. If the increase of positive electrical potential due to the ions exceeds the electrical resistance limitation of the intracellular negative electrical potential, the cell membrane is locally disrupted resulting in pore formation [30, 31]. Using electroporation,

[a] *Department of Mechanical Engineering, Kyushu University, Fukuoka 819-0395, Japan. Tel: +81-92-802-3156; E-mail: Yoko@mech.kyushu-u.ac.jp*
[b] *Bioproduction Research Institute, The National Institute of Advanced Industrial Science and Technology (AIST), Ibaraki 305-8566, Japan. Tel: +81-29-861-2641; E-mail: shigeo.sugano@aist.go.jp.*
†Electronic Supplementary Information (ESI) available. See DOI: 10.1039/x0xx00000x

2.9–12.6-kbp plasmid DNAs, were delivered into Bacillus subtilis ISW1214 with the same efficiency with varied electric fields with strength up to 28 kV/cm and pulse duration of 500 μs [32]. In addition, it has been reported that the waveforms of the voltage pulse affect the charged groups of the membrane (e.g., phosphate head groups of lipid molecules), and open holes in the cell membrane [33]. Notably, electrical pulses can produce membrane pores in the range 1–100 nm using this method [34]. Although electroporation is applicable for varied cell types, it is still challenging to transfecting large molecules with high-volume genomic information. Therefore, a physical method applicable to a variety of cell types such as osteoblasts and microalgae is highly desired.

In this study, we demonstrate unprecedented electromechanical poration using a core-shell-structured microbubble generator, comprising a fine microelectrode covered with dielectric material. By introducing a microcavity at its tip, we concentrated the electrical field with respect to the applied repetitive electric pulses and generated microbubbles. The microbubble generator offers two important contributions. One is the electrical stimulus. The electric field was calculated to be several MV/m at the tip of the bubble generator, comparable to the level of electric field used in the electroporation method [35-37]. As shown in Fig. S1, for a bubble generator made from a tungsten wire and a Teflon tube, the electric field was concentrated at the tip. Cell suspension at the position 100 μm from the tip might be exposed to an electric field of 1 MV/m. The electric field decreased drastically as the distance from the tip increased. We anticipate similar mechanisms to electroporation, where the positive electric field excess within the cell membrane is induced by the concentrated electrical field, and results in poration. The other is the mechanical stimulus, which is a unique feature of our method. The repetitively generated microbubbles apply different degrees of mechanical stimulation in the cell suspension owing to their behavior, including fluidic oscillation caused by their expansion/contraction and shock waves caused by their collapse. Moreover, the behavior can be controlled not only by changing the strength and frequency of the applied electrical pulses but also by changing the viscosity of the cell suspension. We experimentally optimize the electrical pulses and viscosity using the transfection efficiency and show the transfection of large molecules (thousands of kDa) into osteoblast-like cells and Chlamydomonas, which are generally considered to be difficult to inject. Notably, we find that the transfection efficiency can be enhanced by increasing the viscosity, though the details of the underlying intracellular delivery mechanism are currently unclear. The applicability of the technology to a variety of cell types opens up numerous bioengineering applications.

Results

Proposed mechanism of electromechanical poration

Fig. 1 shows a proposed mechanism of the electromechanical poration method based on the core-shell-structured microbubble generator. The generator comprises a microcavity at the tip of the generator, which is configured between the fine core of the active electrode and outer dielectric shell (Fig. S2). The bubble generator and an opposing electrode are introduced into a cell suspension containing target molecules. When electrical pulse signals are applied between the electrodes, an electrical field is finely concentrated at the tip of the injector[35, 36], which results in the rapid generation of microbubbles in the suspension. The suspension viscosity is artificially tuned to control the mechanical stimuli, which trigger the remodeling of the cell membrane. Fig. 1a depicts what happens in electromechanical poration with respect to the viscosity of the cell suspension. When the microbubbles are electrically generated, the cell suspension surrounding the generator tip behaves in one of two ways depending on the viscosity of the cell suspension, and the fluidic behaviour cause different degrees of mechanical stimulation of the cells in suspension (Fig. 1b). In the case of low-viscosity suspensions, the generated bubbles are sequentially released owing to the jet flow induced by bubble expansion. As a result, the cell suspension circulates in the culture container. Because cells, therefore, move as part of the circulating flow, they are mainly exposed to the relatively small mechanical stimulus of fluidic shear force in terms of the microscopic perspective. In the case of high-viscosity suspensions, the jet flow does not result from the bubbles generated by the electrical pluses. In this case, the bubbles expand and contract repeatedly at the tip of the injector. Stagnant bubbles occur. The reason is supposed to be that as the viscosity increases, the drag force induces by samples becomes higher, which hinders the release of microbubbles. To instinctively demonstrate how sample viscosity leads to stagnant bubbles at generator tip, we conducted experiments using samples with 0 to 25% (v/v) thickener (long cellulose nanofiber fibers (LCNF)). The viscosity increased as the thickener concentration increased [38]. As shown in Movies S1 to S4, the bubbles were released from the tip of the bubble generator in samples with 0, 5, 10 and 15% LCNF. As the viscosity further increased, oscillating (stagnant) bubbles were observed in samples with 20% or 25% LCNF (Movies S5 to S6). In this study, we propose that high sample viscosity can be achieved by increasing cell or thickener concentration (Fig. 1b). In such high-viscosity suspensions, the fluidic oscillation is transmitted through the suspension, and the cells are exposed to the relatively large mechanical stimulus caused by the pressure oscillation.

Notably, we found that the mechanical stimuli caused by the pressure oscillation trigger remodeling of the membrane cytoskeleton is key to the proposed mechanism underlying the intracellular delivery of the target molecule in electromechanical poration. We hypothesized that the exposure to a mechanical stimulus caused by the

electromechanical poration softens cells in suspension. Fig. 2 shows an example of the morphological changes of cellular actin fibers in NIH/3T3 cells following our poration method, where the viscosity was adjusted using the cell concentration. Before exposure to the pressure oscillation, a dense actin cortical layer was observed below the plasma membrane of cells at low (Fig. 2a) or high (Fig. 2b) concentration. After exposure, the actin layer under the cell membrane was unchanged for the low-viscosity (low-concentration) suspension (3.6×10^4 cells/μL). In contrast, the cortical actin structure largely disappeared for the high-viscosity (high-concentration) suspension (2.1×10^5 cells/μL). In addition, actin stress fibers were observed again following 24 h of culture, post exposure. To confirm that the membrane actin cortex disassembled immediately after 12-W bubble exposure at high viscosity (high concentration), we quantified the distribution of fluorescently labelled F-actin in single cells from the cell periphery to the cell center (areas A1 to A5 in Fig. 2d). We supposed that F-actin disassembly results in re-distribution of stress fibers in single cells. The quantification data (Fig. 2d) suggests that there were no significant differences between untreated cells and cells exposed to 12-W bubbles in low-concentration samples. On the other hand, F-actin signals at cell periphery decreased significantly in high-concentrated cell samples compared to that of the untreated samples. These results indicate that the actin organization of the high-viscosity (high-concentration) suspension was markedly influenced by electromechanical poration, and transfected cells regenerated actin stress fibers after culture. Because the disappearance of actin networks in suspended cells correlated with cell softening [39], this result suggests that exposure to electromechanical microbubbles resulted in the enhancement of cell mechanical properties, which improved the effectiveness of electroporation. In short, we propose that the mechanical stimulation in the case of high viscosities, regulates the cell polarity and the trans-membrane voltage [40], which weakens the cell membrane [41], supporting the pore formation induced by the electric fields (electroporation) between the microbubble generator and the negative electrode.

Effect of varying suspension viscosity using cell concentration

To increase the viscosity of cell suspensions we generally have two choices: increasing the cell concentration and adding thickener. Here, we evaluate the contribution of the cell suspension viscosity, which was controlled by changing the cell concentration. First, we optimized the output powers and cell concentrations to demonstrate the effectiveness of the developed transfection system. We compared the electromechanical poration by varying the output power from 4 to 15 W using cell suspensions containing 2.1×10^5 cells/μL. The GFP expression plasmid (pEGFP-N1, 4.7 kbp) was used as the target molecule so that the transfected cells could be visualized. From Fig. 3, we can see that the number of transfected cells increased when the output power was increased to 12 W. When the output power was further increased to 15 W, the number of transfected cells decreased. A previous study showed that when using the electroporation method, as the field strength increased (0 – 3 kV/cm), cell viability decreased from 100% to approximately 25% [42]. Faurie et al. showed that the transfection efficiency of CHO cells reached a peak at 0.4 kV/cm using electroporation method, but the efficiency decreased significantly from 0.6 to 1 kV/cm. The reason was concluded to be a marked loss in cell viability [43]. To confirm the reason in our study, we measured cell viability under the control condition and at 12 and 15 W (Fig. 3c). The calculation method of cell viability was adapted from a previous study on the electroporation of suspended cells [44]. Briefly, we normalized the cell number of the treated sample to that of the untreated (control) (details are shown in Figs. 3c, S3 and Materials and Methods). The cell viability was approximately 60% at 12 W. On the other hand, the cell viability decreased to approximately 25% at 15 W. Therefore, although more cells may be porated at 15 W compared to 12 W, most of the porated cells may die because of the permanent poration. These results indicated that electromechanical poration involved a trade-off between transfection efficiency and cell viability—similar to that for electroporation—and, of the tested conditions, an output power of 12 W was the most effective for cell injection.

Next, we conducted experiments to determine whether the high-viscosity conditions benefit stress exposure. We evaluated the viscosities of samples with different cell concentrations; 3.6×10^4, 1.1×10^5, 2.1×10^5, and 4.3×10^5 cells/μL using a rheometer (Fig. 4a). The shear viscosity increased with the cell concentration. Note that the shear viscosities of the samples with 2.1×10^5 and 4.3×10^5 cells/μL were higher than that of the control containing only Opti-MEM and plasmids. We observed fluidic behavior caused by microbubble generation. Supplementary Movies S7 and S8 show the typical results for low- and high-viscosity suspensions whose cell concentrations were 3.6×10^4 and 2.1×10^5 cells/μL, respectively. Note that the output power was 12 W in both cases. At low cell concentration, the bubble generator induced free circulating flow (Movie S7). In contrast, at high cell concentration, the microbubbles oscillated intensely, and free circulating flow including cells was restricted (Movie S8). These results demonstrate the effect of viscosity on bubble behavior and indicate that experimental conditions can be optimized to tune mechanical stimuli for molecular transfection. We conducted transfection experiments using pEGFP-N1 plasmid with different concentrations of NIH/3T3 cells (Figs. 4b and 4c). Figs. 4b and 4c show that numerous NIH/3T3 cells were transfected with plasmid pEGFP-N1 at high-viscosity for the cell concentrations 2.1×10^5 and 4.3×10^5 cells/μL, in contrast to at low-viscosities with 3.6×10^4 and 1.1×10^5 cells/μL. These results indicate the effects of cell concentration on transfection efficiency, and

demonstrate our concept for a high-efficiency cell transfection method.

Viscosity-aided cell transformation using thickener

On the basis of the described results, which indicated that the shear velocity of cell suspensions correlated with the transfection efficiency, we evaluated the other method for increasing the viscosity of cell suspensions; adding thickener, which has the advantage of allowing a low concentration cell suspension, extending the potential applications. We investigated molecule transfection to a low cell concentration suspension by adding thickener to a low-viscosity suspension (3.6×10^4 cells/μL) to reconstruct a highly viscous environment. The considerable range of thickeners includes glycerol, cellulose nanofibers (CNFs) [45], and carboxymethyl cellulose (CMC) [46]. We chose to evaluate CNFs and CMC. Adding a small volume of CNFs to the cell suspension gives viscous suspensions because of their high aspect ratio and interfibrillar hydrogen bonds. In addition, CNFs are derived from wood fibers, and therefore have high biocompatibility and biodegradability. CMC is a well-established low-cost material that is chemically synthesized from cellulose that has even higher biocompatibility than CNFs. Although CMC has a lower thickening effect than CNFs, it is already used as a food additive. We evaluated the effect of nanofibers in thickener using two CNFs and a CMC. We used AFo-10002 (short CNF, SCNF) and BMa-10002 (long CNF, LCNF) as different aspect ratio CNFs, and TFo-10002 (fiber-type CMC with 10 μm cross-sectional diameter) as the CMC (see Materials & Methods).

First, we assessed the viscosity changes induced by adding the thickeners (Fig. 5a). As anticipated, the viscosity of the cell suspension increased in each case. Additionally, the thickening effects on the shear viscosity for the high aspect ratio was greater than that of the shorter CNFs. Note that the viscosity of CMC (no CNFs) with a concentration of 45% (CMC-45%) was comparable to that of BMA/-10002 cellulose long with a concentration of 7% (LCNF-7%) (Fig. 5b). In addition, the transfection efficiency improved up to approximately 16.8%, 36.1%, and 9.1% for SCNF-21%, LCNF-21%, and CMC-45%, respectively (Fig. 5c). The transfection efficiency improved in each case, and higher viscosities gave higher transfection efficiency. In addition, prominent morphological change of NIH/3T3 cells was not observed (Fig. S4a). The cell viability of samples with the addition of 21% LCNF was not changed significantly compared with the control samples (Figs. 5c and S5). The thickener, therefore, might have biocompatibility. After transfection using the electromechanical poration method at 12 W, the cell viability of samples with 21% LCNF was in the range of 50% to 80% when the transfection efficiency was approximately 30% (Fig. 5c). These results imply that the sample viscosity is a key factor in promoting cell transfection through microbubbles.

Applicability to a variety of cell types

The proposed electromechanical poration method offers a wide range of opportunities for transfecting cells with molecules resulting in high viability as it softens the target cell using convenient mechanical stimuli. In this study, we demonstrate two examples of molecule transfection. First, we conducted experiments using a rat osteosarcoma cell line, UMR-106 cells, at different concentrations or with the addition of CNFs. UMR-106 is used as a model of bone-forming and bone-remolding cells, which recapitulate bone regeneration and vitamin D signaling. pEGFP-N1 was the target molecule for transfection. In this study, high cell concentration was determined based on the viscosity, at a level of which oscillating bubbles occurred at the tip of the bubble generator. Therefore, we investigated the viscosity of cell samples. As shown in Fig. 6a, the viscosity of UMR-106 cells with a concentration of 2.1×10^5 cells/μL was higher than that of low-concentration sample (3.6×10^4 cells/μL). The viscosity level was as low as 10^{-3} Pa·s (the viscosity level of OPTI-MEM or water). In addition, we observed oscillating bubbles in the high-concentration sample of UMR-106 cells (Movie S9). Therefore, we used two high-viscosity suspensions achieved through high cell concentration (2.1×10^5 cells/μL) and by adding thickener (LCNF-21%). Note that a low-viscosity suspension with 3.6×10^4 cells/μL was used as a control suspension. The transfection efficiency was approximately 45% in the case of the high-concentration suspension (Fig. 6b), which was higher than that of the low-concentration suspension. The transfection efficiency was also up-regulated to approximately 36% for the sample with thickening agent (Fig. 6b). Further, it seems that there were no prominent morphological changes of UMR-106 cells after the addition of 21% LCNF (Fig. S4b). Addition of 21% LCNF only did not result in significant decrease of cell viability (95 ~ 100% cell viability with the addition of 21% LCNF, Figs. 6c and S6). These results indicate that LCNF might have biocompatibility. After transfection using the electromechanical poration method at 12 W, the cell viability of the 21%-LCNF sample was in the range of 50% to 80% when the transfection efficiency was approximately 50%. The results indicate that electromechanical poration has the potential to be used for transfection of various cell types. Next, we conducted experiments on *Chlamydomonas reinhardtii* to further demonstrate the versatility of electromechanical poration. Although Chlamydomonas is a microalga that has been suggested as a future source of renewable biofuel [47], it is difficult to manipulate genes in Chlamydomonas because of its rigid cell wall [48]. Similarly, we also investigated the viscosity of samples to determine the low-/high-concentration samples. The viscosity of low-concentration (3×10^5 cells/μL) *Chlamydomonas* was comparable to that of low-concentration UMR-106. Further, the viscosity of high-concentration (7.5×10^5 cells/μL) sample was slightly larger than that of high-concentration UMR-106. Cells with no green fluorescence were observed in samples under static conditions. 2000-kDa FITC-dextran (estimated

hydrodynamic diameter: 54.4 nm) [49] was delivered into only a few cells in a cell suspension with 3×10^5 cells/μL. At 7.5×10^5 cells/μL, the transfection efficiency of FITC-dextran was increased to more than 40% (Fig. 6d). The cell viability of Chlamydomonas was in the range of 60% to 80% after 24-h incubation (12-W bubble treatment). Thus, the system is applicable to the delivery of macromolecules to cells with cell walls, and the sample viscosity is a crucial parameter for transfection even in plant cells. Because FITC-dextran has been used to evaluate the membrane permeability of cell membranes for transfection [50], the results directly demonstrate that the developed electromechanical method induced pore formation after microbubble exposure.

Delivery of plasmids with different size

We evaluated the possibility of delivering large plasmids. Plasmids of different sizes up to 15 kbp were successfully transfected into UMR-106 cells, as large cargo models containing high-volume genomic information (Fig. 7b). The transfection efficiency of 11 kbp plasmid to UMR-106 cells was approximately 8% using the electromechanical poration system (Fig. 7c). This result suggests that the transfection efficiency of large molecules into cells depends on the molecular size.

The adhered cells decreased as the size of plasmid increased (Fig. 7c). The reason might be that large-size plasmid is toxic to cells when exposed to physical stimulation [51]. To test whether cells subjected to oscillating microbubbles can proliferate, we conducted cell selection experiments following the delivery of plasmids using the vector harboring both GFP and RFP-2A-PURO expressing cassettes (the plasmid pCDH-GFP-RFP-PURO with a size of 8.3 kbp used in Fig. 7c). After transfection using the electromechanical poration method, cells with both GFP and RFP expression were observed at 24 h (Fig. 8). Note that we used lipofection, which is widely used for transfecting cells with molecules, to evaluate the effectiveness of the proposed method. UMR-106 cells grew to confluence after gene delivery using either lipofection or electromechanical poration. The number of GFP- or RFP-expressing cells increased after treatment with puromycin for 48 h, which suggests that the transfected cells proliferated and their descendants also expressed the PURO gene (Fig. 8). In contrast, non-transfected cells were killed by the puromycin treatment. At 48 h after puromycin treatment, GFP was expressed in approximately 99% of both samples, transfected using lipofectamine or the electromechanical poration method (Fig. 8). Notably, the transfection efficiency of UMR-106 using the electromechanical poration method was higher than that of the lipofection method, as shown in Fig. 9. These results confirmed that the cells transfected with the antibiotic-resistant cassette using electromechanical poration, exhibited similar proliferation status in response to antibiotics to those transfected using the conventional method.

Discussion

The results described demonstrate the effectiveness of our system for delivering cargos. In this section, we discuss the mechanisms underlying its delivery of large molecules into cells. Based on previous studies, the mechanisms underlying cell transfection by electroporation are as follows [52-56]. 1) An electric field using high intensity electrical pulses is applied to cells. 2) The trans-membrane voltage increases rapidly, attracting small conducting ions (e.g Na+ and Cl−) from the surrounding medium [52, 53], . The cell membrane transits from an insulating state and becomes conductive [53]. When the capacitance of the membrane is exceeded, the lipid-bilayer rearranges and pores are formed in the cell membrane. 3) The changes in mechanical force within the membrane lead to an expansion of membrane pores for the cellular uptake of biological molecules. The pore formation has a time range of ns to μs [53]. In addition to the described poration mechanism, we observed changes in the structure under the cell membrane after exposure to electrically induced microbubbles using our system (Fig. 2). Although the electric field at the tip of the microbubble generator might be involved in decreased cell viability (Fig. S1), we noticed that exposure to 12-W power did not result in prominent cell transfection in low-concentration cell suspension, which demonstrated that the electric field without oscillating microbubble could not increase cell transfection. Based on these observations, our proposed mechanism for electromechanical poration is that fluidic oscillation caused by the microbubbles enhances the effectiveness of electroporation by changing the mechanical characteristics of the cell membrane. Although it remains difficult to distinguish the effects of microbubbles and electrical discharge on cell membranes as both are caused by electrical pulses at almost the same time point, our proposed mechanism is based on the underlying electroporation methods and the possible behaviour of microbubbles with the aid of viscosity. The question remains, how does increasing the viscosity enhance cell transfection?

Briefly, because the cell membrane is regarded as a mechano-sensing structure for cells [57], viscosity was used as a key property of the microenvironment to control the mechanical forces related to fluid flow [58, 59], and therefore cell responses. When using electromechanical poration, adjusting the sample viscosity regulated the level of shear stress exerted on suspended cells, and the oscillation of microbubbles in the viscous cell suspension weakened the cell membrane for effective electroporation. In a low-viscosity liquid, a convection flow of the thin liquid was observed when the sample was exposed to microbubbles at 12 W. Because the bubbles were ejected from the tip of the generator, the mechanical forces were transiently dissipated into a wide area (Movies S1-S4 or Movie S7) [60-

[63]. The suspended cells flowed with the fluid without strong resistance [64, 65]. Therefore, the shear stress exerted on cells was extremely low because of mechanical dissipation and low resistance, which can be ignored from a microscopic perspective. In contrast, in a high-viscosity liquid, the viscous drag hinders the ejection of the microbubbles like a damper and the microbubbles cyclically vibrate at the initial position (the tip of the bubble generator). The free movement of cells is also restricted by the viscous microenvironment. The cyclic bubble deformation results in fluid shear stress, which may induce deformation of the cell membrane. Therefore, with the aid of viscosity, the oscillation but not the collapse of microbubbles was applied effectively for membrane deformation here. The effectiveness of oscillating bubbles on cell poration was also confirmed by using bubbles (diameter: ~ 20 μm) driven by acoustic fields [66]. Previous studies reported that the periodic succession of attractive and repulsive forces induced by an oscillating air microbubble adsorbed on the wall of a cuvette [67, 68] resulted in the deformation or disruption of giant unilamellar lipid vesicles approaching the bubble [66, 69].

In this study, the induced strong mechanical stimuli may promote the delivery of large molecules into cells by overcoming the cell membrane barrier. Differences in the mechanical properties of the cell membrane—such as reduced thickness and changes in the conformation/bending stiffness—after mechanical stimuli, were demonstrated in previous studies [41, 70, 71]. Actin forms one of the cell cytoskeletons that regulate cell mechanics. A previous study showed that the morphology of the cortical actin structure underneath the plasma membrane of suspended cells is related to the mechanics (stiffness) of the suspended 3T3 cells [39, 72]. The reduction in actin structures underneath the cell membrane was related to lower cell stiffness [39]. Furthermore, we showed that NIH/3T3 cells responded rapidly to microbubble exposure by remodeling the actin structure below the cell membrane (Fig. 2). The results for the delivery of 2000-kDa FITC-dextran into Chlamydomonas suggested the high permeability of the cell membrane resulted from the electromechanical poration (Fig. 6d). Therefore, it is reasonable to suppose that the electromechanical poration method effectively changes the physical properties of the cell and leads to pore formation for the delivery of large molecules. The effectiveness of our electromechanical poration could be dependent on other system parameters or cell type. For example, we found that transfection efficiency in UMR-106 cells was higher than that in NIH/3T3 cells (Figs. 3a and 9), whereas NIH/3T3 cells are known to be one of the easiest-to-transfect cell lines and UMR-106 is not. For the transfection of NIH/3T3 cells, there are parameters to be optimized such as the relationship between the size of the bubble generator and the volume of the cell suspension, the number of cycles of bubble exposure and the position of the bubble generator. Meanwhile, we note that UMR-106 continuously secretes a large number of glycoproteins, a type of protein with high intrinsic viscosity, to form bone extracellular matrix [73]. In terms of the principle of electromechanical poration, the amount of extracellular matrix, which potentially inhibits cell movement inside the reactor, would be a possible factor in transfection efficiency.

Materials and Methods

Core-shell-structured microbubble generator and experimental system configuration

The core-shell-structured bubble generator was fabricated using a tungsten wire with 100-μm cross-section, a Teflon tube (inner diameter 100 μm, outer diameter 300 μm), an intravenous (IV) indwelling catheter, and an electrode. The tungsten wire was approximately 5 mm longer than the Teflon tube. After insertion into the Teflon tube, the end of the tungsten wire was inserted into the tip of the indwelling catheter (a slender stainless steel tube) to form an electrode. The detailed fabrication process is shown in Fig. S2. When a single pulse with a peak voltage of 500 V was applied to the generator and the negative electrode, the microbubbles grew to a maximum size (sub-millimeter) within 5 μs (Fig. 10 and Movie S10). The system used for transfection consisted of a power source (Hyfrecator 2000, ConMed Corporation, USA), two micro-manipulators (QP-2RLH-PC, Micro Support Co., Ltd., Japan) and a bubble injector (Fig. 10). The Bipolar (BI) mode was used, and the power could be adjusted from 0 to 35 W. A signal from the PC was used to trigger the power source through a digital I/O unit. 600 pulses were generated in approximately 0.018 s at each trigger when the power source was externally triggered once [74]. Each power unit was triggered 30 times. An oscilloscope was used to monitor the voltage and current during the experiments. The injection position was changed randomly within 500 μm in the x–y plane by the micromanipulator after each trigger signal, and the time interval between signals was 2 s.

Cell culture and application of FITC-dextran and plasmids

NIH/3T3 (CRL-1658) and UMR-106 (CRL-1661) were obtained from the American Type Culture Collection (ATCC) (Manassas, Va., USA). *Chlamydomonas reinhardtii* CC-125 wild type mt+ 137c was used for transformation. NIH/3T3 and UMR-106 were cultured in high-glucose Dulbecco's Modified Eagle's Medium (DMEM) (ATCC 30-2002, Manassas, Va., USA) containing 10% heat-inactivated fetal bovine serum (Austral Biologicals, USA), and 1% penicillin and streptomycin (Invitrogen). The cell lines were maintained at 37°C under 5% CO2 in a humidified atmosphere and grown to confluence. Wild-type Chlamydomonas was grown on a tris-acetate-phosphate

(TAP) solid medium containing 1% agar in a 100-mm dish. Chlamydomonas was cultured under continuous illumination (82 µmol photons/m2s) at 22°C.

We used 2000-kDa fluorescein dextran to evaluate the effectiveness of the electromechanical poration to deliver large molecules into Chlamydomonas [75]. The volume of the cell suspension for transfection was 7 µL. The final concentration of the fluorescein dextran was approximately 85 µg/µL. We used plasmids in the experiments transfecting NIH/3T3, UMR-106, and MSC. The pEGFP-N1 plasmid DNA (4.7 kbp) (Chlontech, #6085-1), pCDH-GFP-RFP-PURO (8.3 kbp) [76], MS2-P65-HSF1 (11 kbp) (Addgene, #61423), and pHRdSV40-NLS-dCas9-24xGCN4-NLS-P2A-BFP-dWPRE (15 kbp) (Addgene, #60910) were also prepared using a plasmid Giga prep kit (QIAGEN). Plasmid concentrations of 3–10 µg/µL were used. In the preliminary experiments, cell samples (µL) were transfected with 3.8 (0.54 µg/µL) or 0.9-µg (0.13 µg/µL) plasmid (Fig. S7). We added 15 µg of plasmid to each sample based on the maximum transfection efficiency obtained from experiments using plasmids at different levels (Fig. S7). Exposure to the microbubbles and electric field for 30 triggers did not result in plasmid damage at 12 W (Supplementary method 1 and Fig. S8).

Sample preparation and viscosity measurement

Cell suspension samples formed on the bottom of 1.5-mL microtubes were prepared by centrifugation (Supplemental method 2). Thickening agents BiNFi-s used were purchased from SUGINO MACHINE LIMITED (Toyama, Japan). Thickening agents with cellulose nanofibers (CNFs) or carboxymethyl cellulose (CMC) were used. BiNFi-s cellulose long (LCNFs, BMa-10002) and BiNFi-s cellulose short (SCNFs, AFo-10002) were used. The thickening agent CMC (TFo-10002) was also used. After cells were centrifuged, the supernatant was discarded. Thickening agent with the desired volume was added to cells. Then, Opti-MEM was added to adjust the total volume to 7 µL. The fluid mechanics were investigated using a parallel-plate rheometer Physica MCR 301 (Anton Paar, Australia), which was also used to measure the dynamic viscoelastic properties of the samples with a high cell concentration. We used a CP25-0.5 measuring plate because it only required a small volume of cell suspension (~50 µL). A constant-temperature water bath with a circulating flow of water was used to maintain the temperature at 25°C.

Evaluation of cell viability and cell transfection

Cell (NIH/3T3 or UMR-106) viability was calculated using a protocol adapted from Haberl et al. Briefly, first, the bubble-treated cell suspension was cultured in cell culture dish for 24 h. Then the cells were washed with PBS (-) to remove the floating dead cells. Next, phase-contrast images were collected from 5 random locations using 10× objective (Figs. 3c, S3, S5 and S6). The cell number in the 5 images was counted and normalized to that of the control sample as the relative cell viability of the sample [44].

Cells transfected with plasmid DNA were observed using a fluorescence microscope (Eclipse Ti, Nikon Corporation, Japan) after transfection for 48 h. Images were collected using a 20× magnification lens (L Plan, SLWD 20×/0.35, OFN25, WD 24, Nikon, Tokyo, Japan). The exposure time was 600 ms based on the saturation of the images on day 2. The transfection efficiency was measured using a Countess II FL automatic cell counter (Invitrogen, Massachusetts, USA).

For the measurement of cell viability of Chlamydomonas, samples with a concentration of 7.5×10^5 cells/µL (high concentration) were used. Cells were treated with 12-W microbubbles. After 24-h incubation, Chlamydomonas were staining with FDA (Dojindo), which shows live cells with green fluorescence. For a sample, 5 images were collected at 5 random locations. Cell viability was equal to the percentage of FDA-positive cells with respect to the total cell number in the 5 images.

After the Chlamydomonas suspensions with 2000-kDa FITC-dextran were treated with 12-W bubbles, the cells were centrifuged and washed three times using the TAP medium. Then cells on the glass-bottom dish were imaged in confocal mode using a TCS SP8 confocal laser microscope (Leica) with a 60×/1.2 NA oil objective (Leica). Cells were imaged from dish bottom to top with a step size of 0.3 µm. We counted the cells with FITC-dextran within the cell body using the confocal images collected using the SP8 confocal microscopy. Then the transfected cell number was divided by the total cell number to obtain the value of transfection efficiency of Chlamydomonas.

For cell selection experiments, we transfected UMR-106 cells with pCDH-GFP-RFP-PURO (8.3 kbp), which is a plasmid with a gene for puromycin resistance. Puromycin (InvivoGen, USA) was added to the culture medium of UMR-106 at 24 h to give a final concentration of 20 µg/mL. Following the addition of puromycin for 48 h, the samples were observed and cells were collected using 0.25% trypsin. The percentage of plasmid-expressing cells was measured using Countess II FL.

Cell staining with phalloidin and image analysis

Actin of suspended cells was stained using a method described in a previous study by Chan et al [72]. Briefly, we washed the suspended cells with prewarmed PBS (-) and fixed the cells in the suspended state at room temperature with 4% paraformaldehyde phosphate buffer solution for 20 min. Then, we incubated the suspended cells with 0.1% Triton X-100 for 5 min. Subsequently, we stained the cells by incubating the fixed cells with phalloidin-Alexa-Fluor 555 (Life Technologies) for 20 min in the dark. The sample was then washed three times with PBS (-). Actin of cells cultured for 24 h was stained using a similar protocol. Cells stained for actin were imaged in confocal mode using a TCS SP8 confocal laser microscope (Leica) with a 40×/1.2 NA oil

objective (Leica). Cells were imaged from bottom to top with a step size of 0.35 µm. Gain settings and exposure times were kept the same for all samples. The intensity of each cell in each image was calculated and the maximum was regarded as the intensity of actin within a cell. We quantified fluorescence intensity of F-actin using ImageJ (NIH). As shown in Fig. 2d, we divided the cell area into five areas with a width of $R/5$ (R was half of the width of a cell with a round shape (i.e., the radius of the cell)). Then the gray value of each donut-shaped area and the center area were normalized to that of the whole cell area to remove the influences of the background and cell individual differences.

Statistical analysis

Results are from 3–6 independent experiments. Differences were examined using one-way repeated measures ANOVA based on the results of normality tests, and a Tukey test was used as the post-hoc analysis method. Results are graphically represented using box charts with boxes determined by the 25th and 75th percentiles. A p value of <0.05 was considered statistically significant. Statistical analysis was conducted using OriginPro 2021.

Author Contributions

YY and SSS conceived the idea of transfection using electrically induced microbubbles and supervised it. SS and WH contributed to the development of the concept of the study. SSS, YY, and WH established the microbubble generation system for the transfection of suspended cells in a microtube. SS, SSS, NT and WH designed the experiments to clarify the underlying mechanisms of the method including the investigation of the effects of cell concentration and the changes of the cytoskeleton underneath the cell membrane. WH and NT measured the viscosity of the cell suspensions. The transfection experiments using various cell types were designed by SSS, YY, and WH. WH, NT, and SSS performed the experiments. WH, SSS, NT, SS, and YY analyzed the data. YY, SSS, WH, and SS contributed reagents, materials, and analysis tools. WH, SS, SSS, NT and YY wrote and revised the paper.

Conflicts of interest

YY, SSS, and WH are inventors of a patent related to this work (serial number: PCT/JP2020/035332) filed on 17 September 2020 filed with the U.S. Patent Office. The authors declare that they have no other competing interests.

Acknowledgements

This work was supported by Core Research for Evolutional Science and Technology (CREST), found by Japan Science and Technology Agency (JST) (JPMJCR19S6). We are grateful to Dr T. Takahashi at Saitama University for providing Chlamydomonas materials and to Professor Yoshinori Sawae and Mr. Hironori Shinmori for their support in the measurements of sample viscosity.

References

1. E. De Vuyst, M. De Bock, E. Decrock, M. Van Moorhem, C. Naus, C. Mabilde and L. Leybaert, *Biophysical Journal*, 2008, **94**, 469-479.
2. Y. Chen, J. Wang, X. Li, N. Hu, N. H. Voelcker, X. Xie and R. Elnathan, *Advanced Materials*, 2020, **32**, 2001668.
3. J. Wu, Y. Shi, X. Pan, S. Wu, R. Hou, Y. Zhang, T. Zhong, H. Tang, W. Du, L. Wang, J. Wo, J. Mu, Y. Qiu, K. Yang, L.-K. Zhang, B.-C. Ye and N. Qi, *Cell Reports*, 2021, **34**, 108761.
4. K. Takahashi and S. Yamanaka, *Cell*, 2006, **126**, 663-676.
5. A. A. Davis, M. J. Farrar, N. Nishimura, M. M. Jin and C. B. Schaffer, *Biophys J*, 2013, **105**, 862-871.
6. H. Yin, K. J. Kauffman and D. G. Anderson, *Nature reviews. Drug discovery*, 2017, **16**, 387-399.
7. K. Chen, Y. Wang, R. Zhang, H. Zhang and C. Gao, *Annual review of plant biology*, 2019, **70**, 667-697.
8. G. Chu, H. Hayakawa and P. Berg, *Nucleic Acids Res*, 1987, **15**, 1311-1326.
9. C. Luft and R. Ketteler, *J Biomol Screen*, 2015, **20**, 932-942.
10. T. Geng, Y. Zhan, J. Wang and C. Lu, *Nature Protocols*, 2011, **6**, 1192-1208.
11. Y. Furuhata, A. Sakai, T. Murakami, M. Morikawa, C. Nakamura, T. Yoshizumi, U. Fujikura, K. Nishida and Y. Kato, *Scientific Reports*, 2019, **9**, 2163.
12. P. Mukherjee, S. S. P. Nathamgari, J. A. Kessler and H. D. Espinosa, *ACS Nano*, 2018, **12**, 12118-12128.
13. J. Bouvette, D. N. Korkut, A. Fouillen, S. Amellah, A. Nanci, Y. Durocher, J. G. Omichinski and P. Legault, *BMC Biotechnology*, 2018, **18**, 76.
14. M. P. Stewart, R. Langer and K. F. Jensen, *Chemical Reviews*, 2018, **118**, 7409-7531.
15. T. L. Roth, C. Puig-Saus, R. Yu, E. Shifrut, J. Carnevale, P. J. Li, J. Hiatt, J. Saco, P. Krystofinski, H. Li, V. Tobin, D. N. Nguyen, M. R. Lee, A. L. Putnam, A. L. Ferris, J. W. Chen, J.-N. Schickel, L. Pellerin, D. Carmody, G. Alkorta-Aranburu, D. del Gaudio, H. Matsumoto, M. Morell, Y. Mao, M. Cho, R. M. Quadros, C. B. Gurumurthy, B. Smith, M. Haugwitz, S. H. Hughes, J. S. Weissman, K. Schumann, J. H. Esensten, A. P. May, A. Ashworth, G. M. Kupfer, S. A. W. Greeley, R. Bacchetta, E. Meffre, M. G. Roncarolo, N. Romberg, K. C. Herold, A. Ribas, M. D. Leonetti and A. Marson, *Nature*, 2018, **559**, 405-409.
16. L. L. Lesueur, L. M. Mir and F. M. André, *Molecular therapy. Nucleic acids*, 2016, **5**, e291.
17. R. Heller, *Science*, 2002, **295**, 277-277.
18. B. Helfield, X. Chen, S. C. Watkins and F. S. Villanueva, *Proceedings of the National Academy of Sciences*, 2016, **113**, 9983.
19. T. D. Xie, L. Sun and T. Y. Tsong, *Biophys J*, 1990, **58**,

13-19.
20. S. I. Sukharev, V. A. Klenchin, S. M. Serov, L. V. Chernomordik and A. Chizmadzhev Yu, *Biophysical journal*, 1992, **63**, 1320-1327.
21. J. Villemejane and L. M. Mir, *Br J Pharmacol*, 2009, **157**, 207-219.
22. W. Wang, W. Li, N. Ma and G. Steinhoff, *Current pharmaceutical biotechnology*, 2013, **14**, 46-60.
23. H. Atkinson and R. Chalmers, *Genetica*, 2010, **138**, 485-498.
24. A. S. Khalil, X. Yu, A. W. Xie, G. Fontana, J. M. Umhoefer, H. J. Johnson, T. A. Hookway, T. C. McDevitt and W. L. Murphy, *Scientific Reports*, 2017, **7**, 14211.
25. X. Du, J. Wang, Q. Zhou, L. Zhang, S. Wang, Z. Zhang and C. Yao, *Drug Deliv*, 2018, **25**, 1516-1525.
26. S. A. Akimov, P. E. Volynsky, T. R. Galimzyanov, P. I. Kuzmin, K. V. Pavlov and O. V. Batishchev, *Scientific Reports*, 2017, **7**, 12152.
27. M. Sun and X. Duan, *Nanotechnology and Precision Engineering*, 2020, **3**, 18-31.
28. D. Peer, *Immunological Reviews*, 2013, **253**, 185-197.
29. T. E. Hartman, N. Sar, K. Genereux, D. S. Barritt, Y. He, J. E. Burky, M. C. Wesson, J. Y. Tso, N. Tsurushita, W. Zhou and P. W. Sauer, *Biotechnology and bioengineering*, 2007, **96**, 294-306.
30. W. Krassowska and P. D. Filev, *Biophysical Journal*, 2007, **92**, 404-417.
31. T. Y. Tsong, *Biophysical journal*, 1991, **60**, 297-306.
32. M. Ohse, K. Takahashi, Y. Kadowaki and H. Kusaoke, *Bioscience, Biotechnology, and Biochemistry*, 1995, **59**, 1433-1437.
33. D. C. Chang, *Biophysical journal*, 1989, **56**, 641-652.
34. T. Batista Napotnik, T. Polajžer and D. Miklavčič, *Bioelectrochemistry*, 2021, **141**, 107871.
35. K. Ichikawa, N. Basaki, Y. Yamashita and Y. Yamanishi, *Micromachines*, 2019, **10**, 389.
36. A. Hirao, K. Miwa, Y. Moriizumi and Y. Yamanishi, 23rd International Conference on Miniaturized Systems for Chemistry and Life Sciences, MicroTAS 2019, Basel, Switzerland, 2019.
37. J. C. Weaver, K. C. Smith, A. T. Esser, R. S. Son and T. R. Gowrishankar, *Bioelectrochemistry (Amsterdam, Netherlands)*, 2012, **87**, 236-243.
38. E. Lasseuguette, D. Roux and Y. Nishiyama, *Cellulose*, 2008, **15**, 425-433.
39. J. Guck, S. Schinkinger, B. Lincoln, F. Wottawah, S. Ebert, M. Romeyke, D. Lenz, H. M. Erickson, R. Ananthakrishnan, D. Mitchell, J. Käs, S. Ulvick and C. Bilby, *Biophysical Journal*, 2005, **88**, 3689-3698.
40. S.-P. Olesen, D. Claphamt and P. Davies, *Nature*, 1988, **331**, 168-170.
41. O. S. Andersen and R. E. Koeppe, *Annual Review of Biophysics and Biomolecular Structure*, 2007, **36**, 107-130.
42. P. J. Canatella, J. F. Karr, J. A. Petros and M. R. Prausnitz, *Biophysical Journal*, 2001, **80**, 755-764.
43. C. Faurie, E. Phez, M. Golzio, C. Vossen, J.-C. Lesbordes, C. Delteil, J. Teissié and M.-P. Rols, *Biochimica et Biophysica Acta (BBA) - Biomembranes*, 2004, **1665**, 92-100.
44. S. Haberl, M. Kandušer, K. Flisar, D. Hodžić, V. B. Bregar, D. Miklavčič, J. M. Escoffre, M. P. Rols and M. Pavlin, *The journal of gene medicine*, 2013, **15**, 169-181.
45. S. Iwamoto, S.-H. Lee and T. Endo, *Polymer Journal*, 2014, **46**, 73-76.
46. X. H. Yang and W. L. Zhu, *Cellulose*, 2007, **14**, 409-417.
47. M. A. Scranton, J. T. Ostrand, F. J. Fields and S. P. Mayfield, *The Plant Journal*, 2015, **82**, 523-531.
48. M. F. Ortiz-Matamoros, M. A. Villanueva and T. Islas-Flores, *Briefings in Functional Genomics*, 2018, **17**, 26-33.
49. H. Chen and E. E. Konofagou, *J Cereb Blood Flow Metab*, 2014, **34**, 1197-1204.
50. G. Chouinard-Pelletier, M. Leduc, D. Guay, S. Coulombe, R. L. Leask and E. A. V. Jones, *BioMedical Engineering OnLine*, 2012, **11**, 67.
51. L. L. Lesueur, L. M. Mir and F. M. André, *Molecular Therapy - Nucleic Acids*, 2016, **5**, e291.
52. J. A. Nickoloff, *Electroporation protocols for microorganisms*, Humana Press, 6th edition edn., 1995.
53. C. Kalli, W. C. Teoh and E. Leen, in *Anticancer genes*, ed. S. Grimm, Springer, 2014, pp. 231-254.
54. J. Gehl, *Acta physiologica Scandinavica*, 2003, **177**, 437-447.
55. J. Weaver, in *Electroporation theory. In: Nickoloff J (ed) Electroporation protocols for microorganisms*, Humana Press, 6th edition edn., 2009, vol. 47, pp. 1-26.
56. C. Chen, S. W. Smye, M. P. Robinson and J. A. Evans, *Medical & biological engineering & computing*, 2006, **44**, 5-14.
57. A.-L. Le Roux, X. Quiroga, N. Walani, M. Arroyo and P. Roca-Cusachs, *Philosophical Transactions of the Royal Society B: Biological Sciences*, 2019, **374**, 20180221.
58. Y. S. Kannan, S. Balusamy, B. Karri and K. C. Sahu, *Experimental Thermal and Fluid Science*, 2020, **116**, 110113.
59. M. Ichihara, H. Ohkunitani, Y. Ida and M. Kameda, *Journal of Volcanology and Geothermal Research*, 2004, **129**, 37-60.
60. D. Kiracofe and A. Raman, *Nanotechnology*, 2011, **22**, 485502.
61. F. Axisa, in *Modelling of Mechanical Systems*, eds. F. Axisa and J. Antunes, Butterworth-Heinemann, 2007, vol. 3, pp. 581-707.
62. A. Yovchenko, S. Bespalko, S. Poliakov, T. Veretilnyk and R. Kapitan, *International Journal of Energy and Environmental Engineering*, 2020, **11**, 485-496.
63. M. S. Longuet-Higgins, B. R. Kerman and K. Lunde, *Journal of Fluid Mechanics*, 2006, **230**, 365-390.
64. P. Singh and D. D. Joseph, *Journal of Fluid Mechanics*, 2005, **530**, 31-80.
65. S. Umeda and W. J. Yang, *Experiments in Fluids*, 1991, **12**, 106-112.
66. P. Marmottant and S. Hilgenfeldt, *Nature*, 2003, **423**, 153-156.
67. P. Marmottant, M. Versluis, N. de Jong, S. Hilgenfeldt and D. Lohse, *Experiments in Fluids*, 2006, **41**, 147-153.
68. P. Marmottant, J. P. Raven, H. Gardeniers, J. G. Bomer and S. Hilgenfeldt, *Journal of Fluid Mechanics*, 2006, **568**, 109-118.

69. B. Dollet, P. Marmottant and V. Garbin, *Annual Review of Fluid Mechanics*, 2019, **51**, 331-355.
70. H. S. Muddana, R. R. Gullapalli, E. Manias and P. J. Butler, *Physical chemistry chemical physics : PCCP*, 2011, **13**, 1368-1378.
71. E. VanBavel, *Progress in biophysics and molecular biology*, 2007, **93**, 374-383.
72. C. J. Chan, A. E. Ekpenyong, S. Golfier, W. Li, K. J. Chalut, O. Otto, J. Elgeti, J. Guck and F. Lautenschläger, *Biophysical journal*, 2015, **108**, 1856-1869.
73. R. J. Midura, D. J. McQuillan, K. J. Benham, L. W. Fisher and V. C. Hascall, *Journal of Biological Chemistry*, 1990, **265**, 5285-5291.
74. K. Ichikawa, S. Maeda and Y. Yamanishi, *Journal of Microelectromechanical Systems*, 2018, **27**, 305-311.
75. S. Bensalem, D. Pareau, B. Cinquin, O. Français, B. Le Pioufle and F. Lopes, *Scientific Reports*, 2020, **10**, 2668.
76. S. Sawatsubashi, Y. Joko, S. Fukumoto, T. Matsumoto and S. S. Sugano, *Scientific Reports*, 2018, **8**, 593.

Figure legends

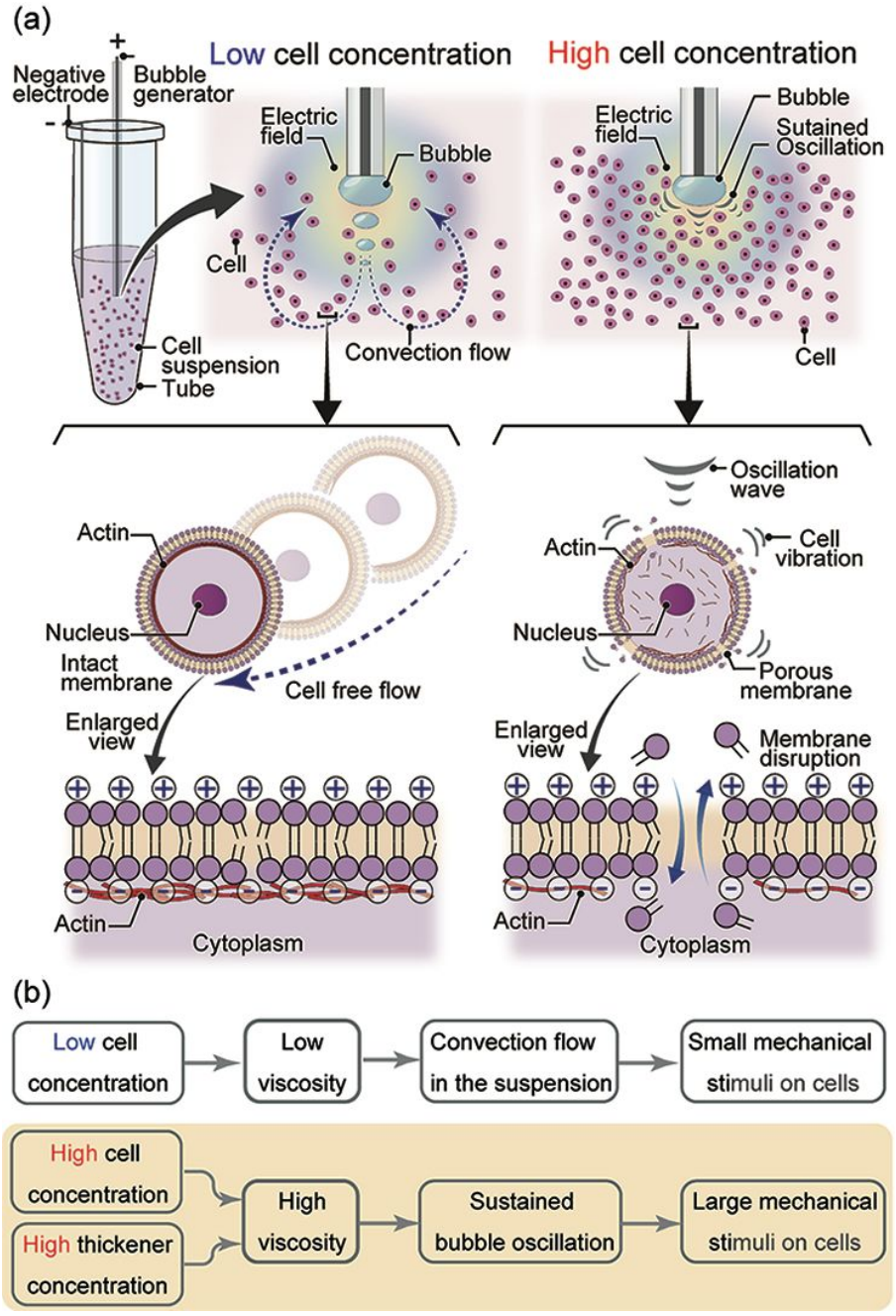

Fig. 1 Concept for cell transfection using bubble generator. The generator system consists of two electrodes. The tips of the two electrodes are inserted into the cell suspension. When the power source generates a voltage pulse, an electrical field forms between the two electrodes and microbubbles are generated. (a) Expected working principles of cell transfection using the bubble generator are as follows. Suspended cells with low or high concentration are simultaneously exposed to both electric fields and shear stress induced by the bubble generator. Cells in a highly concentrated suspension accumulate around the bubble and are exposed to pulsatile shear stress because of the sustained oscillation of the microbubbles. The concentrated environment promotes membrane poration. (b) Proposed methods for the regulation of sample viscosity and mechanical stimuli on suspended cells. The sample viscosity was supposed to influence the mechanical stimulus on suspended cells. Low viscosity is supposed to be related to small mechanical stimuli on cells. On the other hand, high viscosity may result in large mechanical stimuli. There are two possible ways to achieve high sample viscosity for enhanced mechanical stimulus and cell

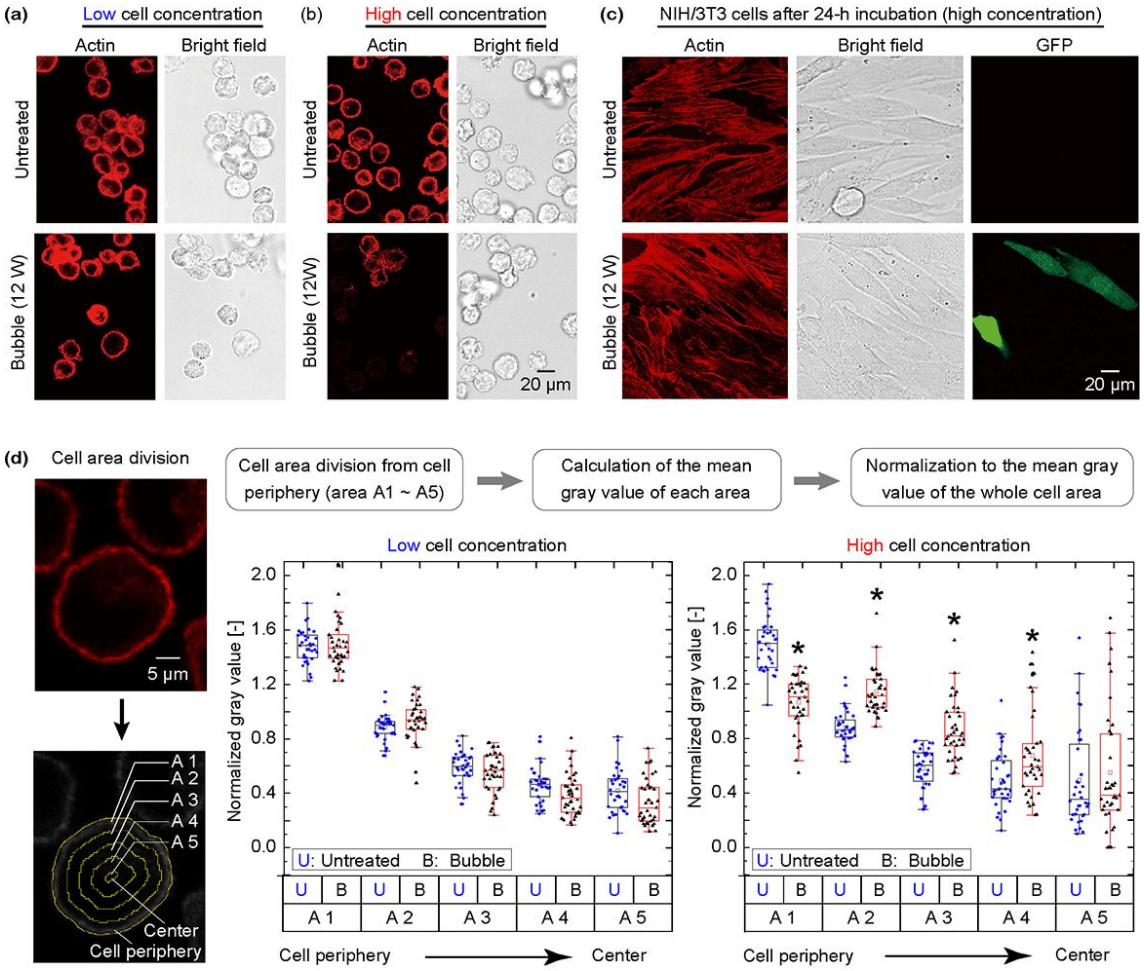

Fig. 2 Cellular response after microbubble exposure. (a) F-actin in cells in low-concentration suspensions with or without the treatment of 12-W bubble. (b) F-actin in cells in high-concentration suspensions with or without the treatment of 12-W bubble. (c) Actin stress fibers in cells seeded onto dishes after microbubble exposure. The actin filament (F-Actin) was stained with Rhodamine-Phalloidin. F-actin was observed in the microbubble-exposed cells after 24-h culture. (d) The calculation results of F-actin distribution in cells at low/high concentrations. A single cell area was divided into 4 donut shaped areas and a center area according to the width of the round cell shape. The gray value of each area was calculated to show the intensity of F-actin. Plasmid pEGFP-N1 (4.7 kbp) was added to all samples in this experiments with a concentration of 2.14 μg / L. Here, no thickener was applied. *: $p < 0.05$ vs. the corresponding

2

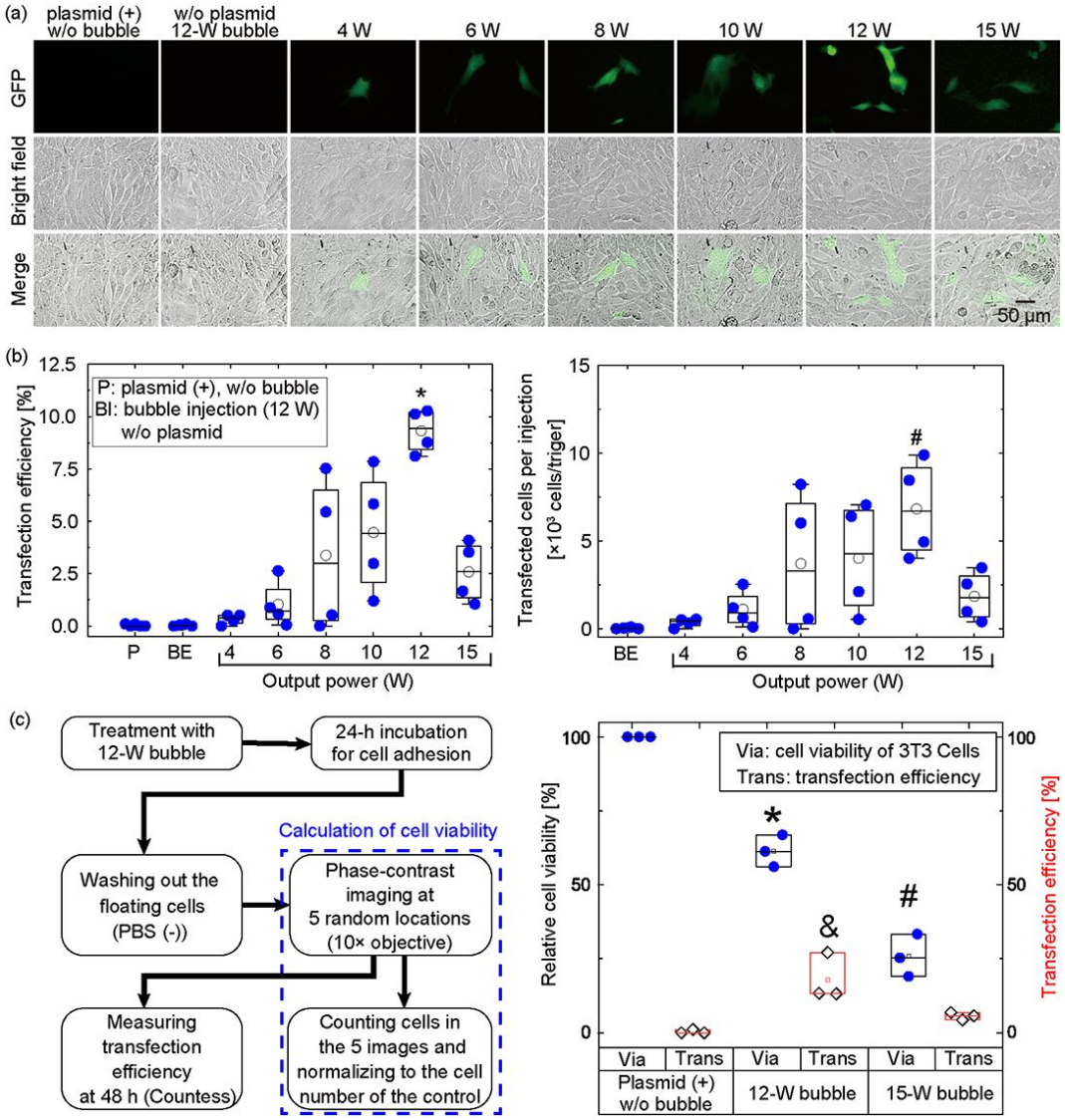

Fig. 3 Effect of output power on transfection efficiency. (a) Representative images of NIH/3T3 cells that were subjected to bubble injection with pEGFP-N1 plasmid at different output powers. Each sample contained 1.5×10^6 cells in a 7-μL suspension (2.1×10^5 cells/μL). Two control samples (plasmid (+), w/o bubble and w/o plasmid, 12-W bubble) were applied. No GFP-expressing cells were observed in the sample without plasmids after bubble injection. Furthermore, without injection, no GFP-positive cells were observed, although plasmids were mixed with the cell suspension. (b) Transfection efficiency at different output powers (left). *: $p < 0.05$ vs. microbubble exposure at 4, 6, 8, 10, or 15 W. The expected transfection events per injection (right). #: $p < 0.05$ vs. microbubble exposure at 4 or 6 W. (c) Calculation of relative cell viability. Cells exposed to microbubbles were incubated for 24 h. The floating dead cells were washed out. Then images of cells were collected from 5 random locations using phase-contrast microscope using 10× objective. The cell count from the 5 images were normalized to that of the control as the relative cell viability [44]. *: $p < 0.05$ vs. control. #: $p < 0.05$ vs. control or 12 W. &: $p < 0.05$ vs. control or 15 W. p values were calculated by using ANOVA in OriginLab 2021.

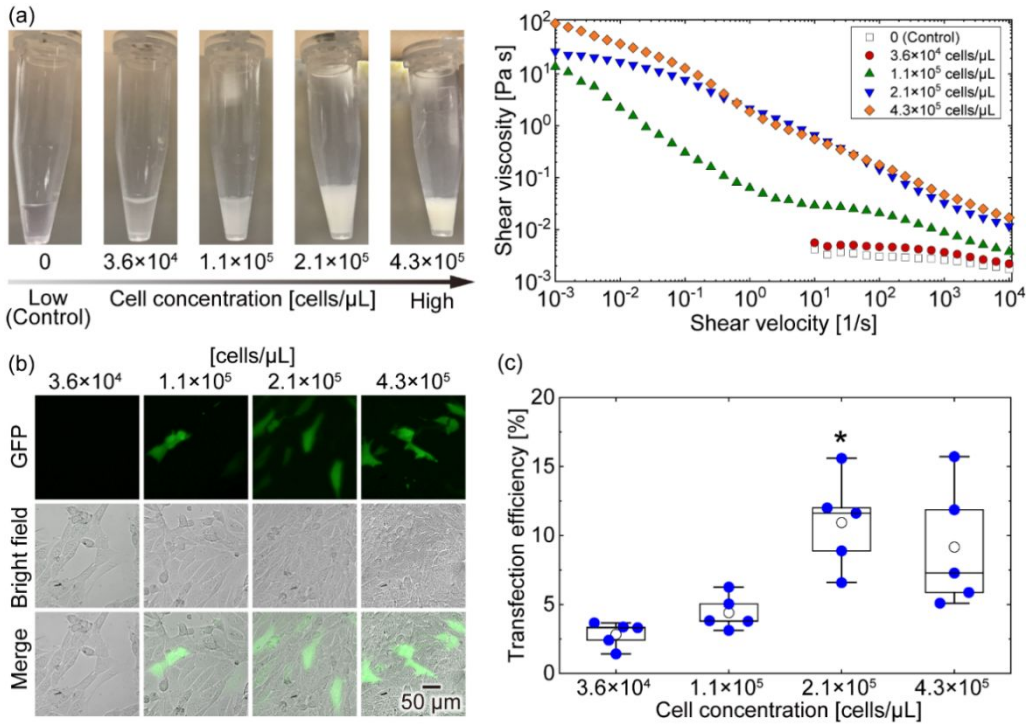

Fig. 4 Effect of cell concentration on the transfection efficiency. (a) Representative images of cell suspensions in microtubes from low to right, respectively). The images show the stocks of cell suspensions with different cell concentration (not the sample for transfection). The samples for bubble exposure were adjusted to be the same as 7μL. Shear viscosity measurements of samples with increased cell concentration (right). Because the viscosities of the sample with 3.6×10^4 cells/μL and the control were lower than the capacity of the measuring plate of the rheometer, the viscosity at shear velocities lower than 10^1 s^{-1} could not be measured. Control indicates no cells added to the medium (OPTI-MEM only). (b) Typical images of NIH/3T3 cells transfected at different cell concentrations. The samples were transfected with plasmid (pEGFP-N1) and images were acquired 24 h after the transfection. (c) Transfection efficiencies of NIH/3T3 cells at different cell concentrations. The electric output power was fixed at 12 W. *: $p < 0.05$ vs. cell concentration at 3.6×10^4 cells/μL. p value was calculated using one-way repeated measures ANOVA with a Tukey test as the post-hoc method.

11

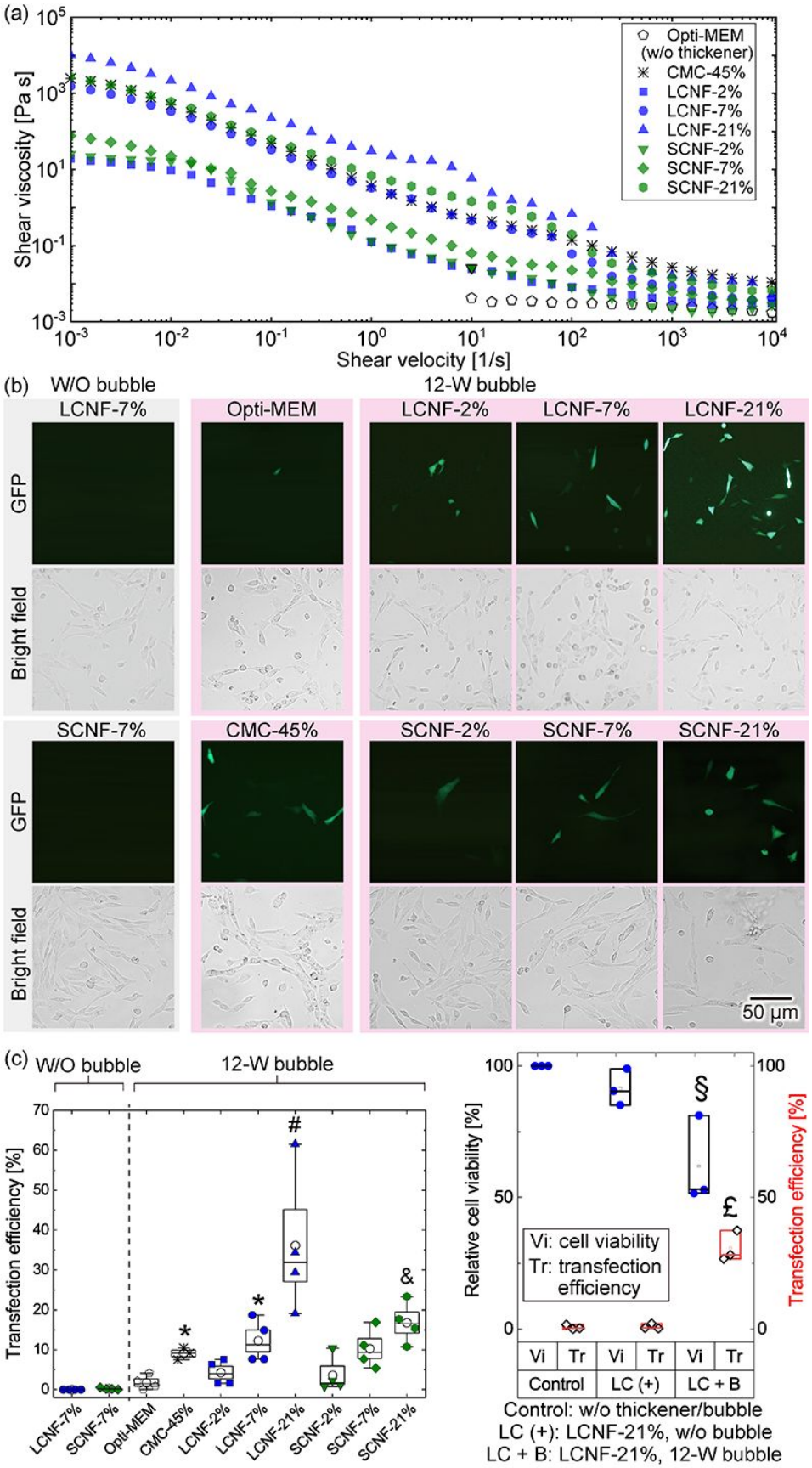
(a)
Shear viscosity [Pa s]
Shear velocity [1/s]
Opti-MEM (w/o thickener)
CMC-45%
LCNF-2%
LCNF-7%
LCNF-21%
SCNF-2%
SCNF-7%
SCNF-21%
(b)
W/O bubble
12-W bubble
LCNF-7%
Opti-MEM
LCNF-2%
LCNF-7%
LCNF-21%
GFP
Bright field
SCNF-7%
CMC-45%
SCNF-2%
SCNF-7%
SCNF-21%
50 μm
(c)
W/O bubble
12-W bubble
Transfection efficiency [%]
LCNF-7%
SCNF-7%
Opti-MEM
CMC-45%
LCNF-2%
LCNF-7%
LCNF-21%
SCNF-2%
SCNF-7%
SCNF-21%
Relative cell viability [%]
Transfection efficiency [%]
Vi: cell viability
Tr: transfection efficiency
Vi
Tr
Control
LC (+)
LC + B
Control: w/o thickener/bubble
LC (+): LCNF-21%, w/o bubble
LC + B: LCNF-21%, 12-W bubble

Fig. 5 Effect of thickeners (cellulose nanofibers (CNFs) and carboxymethyl cellulose (CMC)) on the transfection of NIH/3T3 cells at 12 W. (a) Measurement of the shear viscosity of Opti-MEM with CMC, long CNF (LCNF), and short CNF (SCNF) at different concentrations. (b) Typical images of NIH/3T3 cells transfected in the presence of CNFs and CMC at different concentrations. Plasmid: pEGFP-N1. Opti-MEM: 0.25×10^6 cells/7 μL with Opti-MEM but no CNFs. LCNF-2% (7%, 21%): 0.25×10^6 cells/7 μL with Opti-MEM and 2% (7%, 21%) long CNF. SCNF-2% (7%, 21%): 0.25×10^6 cells/7 μL with OPTI-MEM and 2% (7%, 21%) short CNF. CMC-45%: 0.25×10^6 cells/7 μL with OPTI-MEM and 45% CMC. Static means no bubble injection. (c) Transfection efficiency and relative cell viability in the presence of thickening agents. Control: plasmid (+), w/o thickener/bubble. *: $p < 0.05$ *vs.* Opti-MEM, LCNF-7% (static), or LCNF-2%; #: $p < 0.05$ *vs.* all other samples; &: $p < 0.05$ *vs.* Opti-MEM, SCNF-7% (static), or SCNF-2%. There is no significant difference between LCNF-7% and CMC-45%. §, £: $p < 0.05$ vs. Control or LC (+). p values were

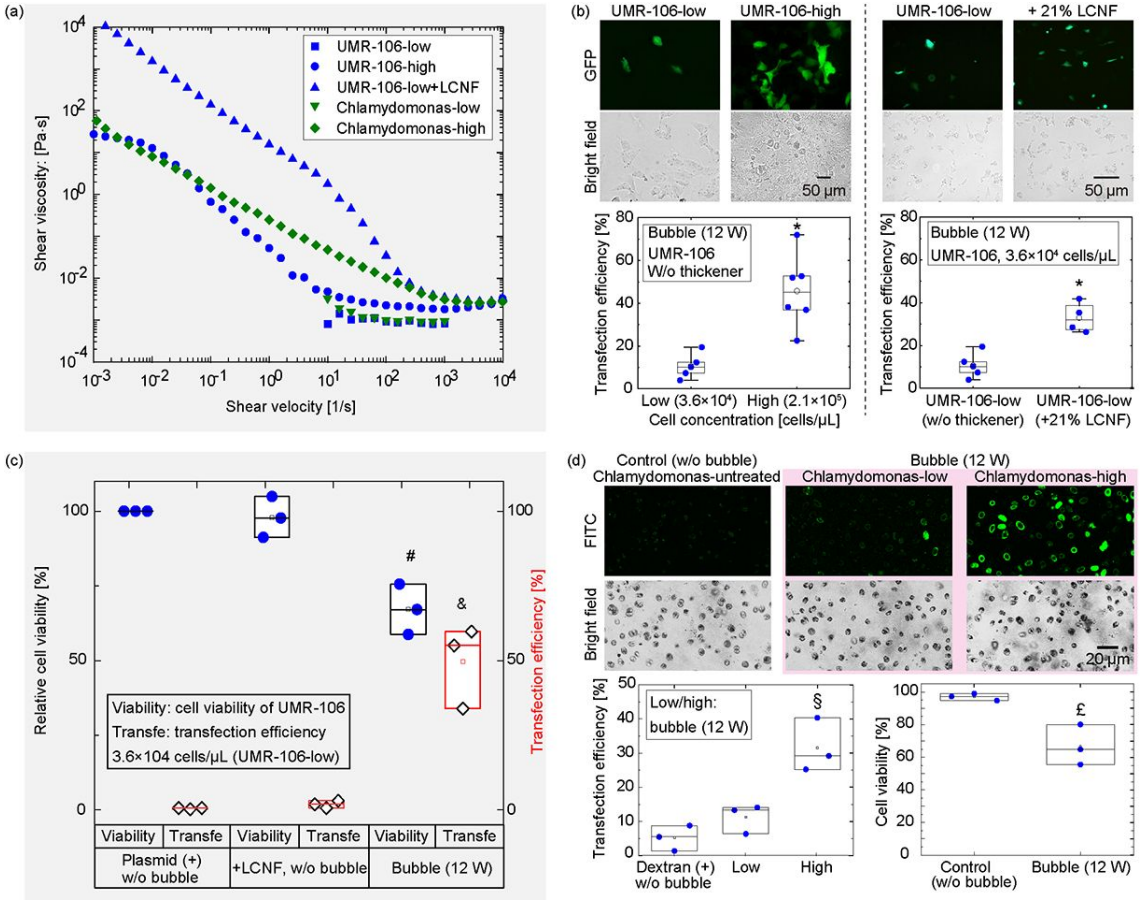

Fig. 6 Effect of cell concentration or adding the thickener (LCNF-21%) on the transfection of various cell types. (a) Measurement of sample viscosity of UMR-106 cells or Chlamydomonas. Here, UMR-low/high is the sample with a concentration of 3.6×10^4/2.1×10^5 cells/μL. Chlamydomonas-low/high is the sample with a concentration of 3×10^5/7.5×10^5 cells/μL. (b) Effect of cell concentration or LCNF on the transfection of UMR-106 cells. *: $p < 0.05$ *vs.* sample with low cell concentration. (c) The relationship between UMR-106 cell viability and cell transfection efficiency with the addition of 21% LCNF. #, &: $p < 0.05$ vs. Control or 21% LCNF. (d) Transfection of *Chlamydomonas* at low/high cell concentration with 2000-kDa FITC-dextran. §: $p < 0.05$ *vs.* Control or Low. £: $p < 0.05$ *vs.* Control (ANOVA using OriginLab 2021).

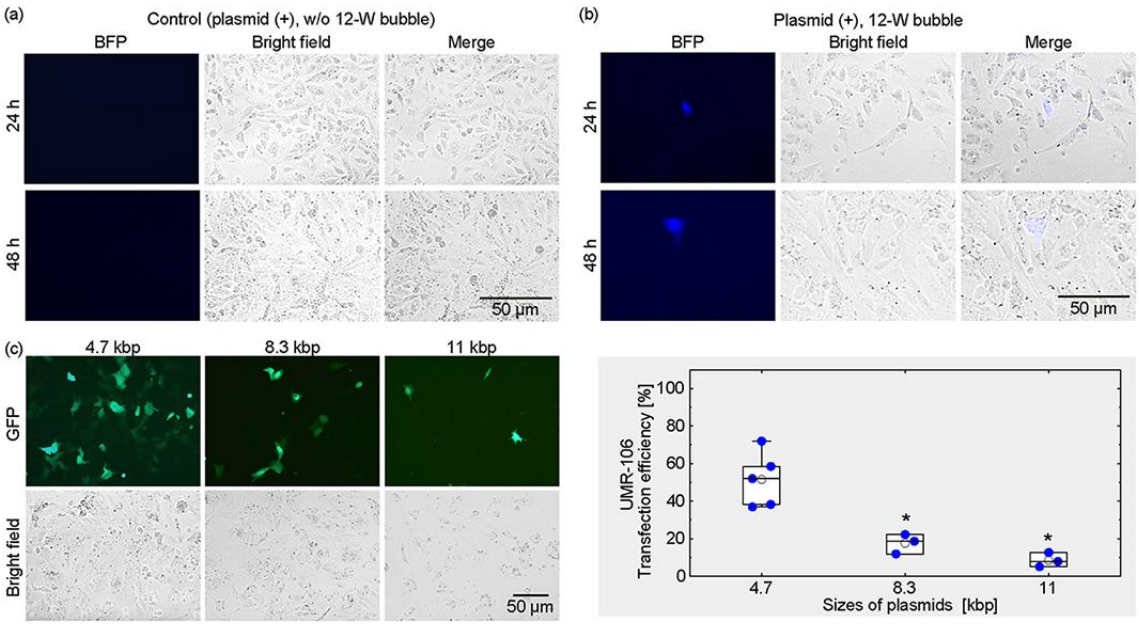

Fig. 7 Assessment of large molecule delivery in UMR-106. (a) A control sample of UMR-106 without the 12-W bubble exposure. (b) Delivery of 15-kbp plasmid (pHRdSV40-NLS-dCas9-24xGCN4-NLS-P2A-BFP-dWPRE) into UMR-106 cells. The cells transfected with plasmid show BFP fluorescence. Images were collected at 24/48 h after transfection. (c) Delivery of plasmids of different sizes (pEGFP-N1: 4.7 kbp; pCDH-GFP-RFP-PURO: 8.3 kbp; MS2-P65-HSF1-GFP: 11 kbp) using microbubbles at 12 W. *: $p < 0.05$ *vs.* 4.7 kbp (ANOVA using OriginLab 2021).

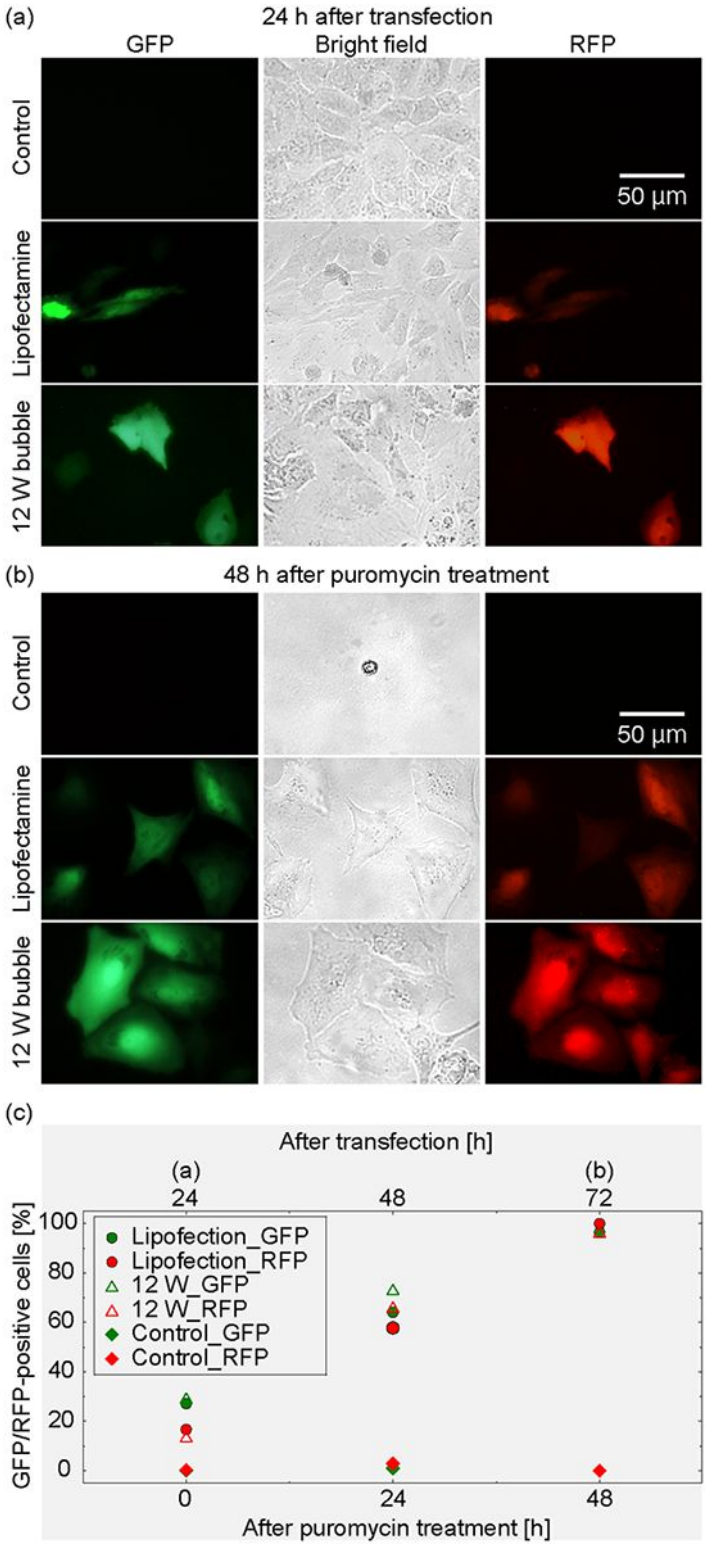

Fig. 8 Cell selection to demonstrate proliferation of the cells transfected using the bubble injection method. (a) Typical images of UMR-106 cells transfected with pCDH-GFP-RFP-PURO harboring a puromycin resistance gene. (b) Typical images of UMR-106 cells after treatment with puromycin for 48 h. (c) Quantification of the ratio of GFP/RFP-expressing cells to non-fluorescent cells during

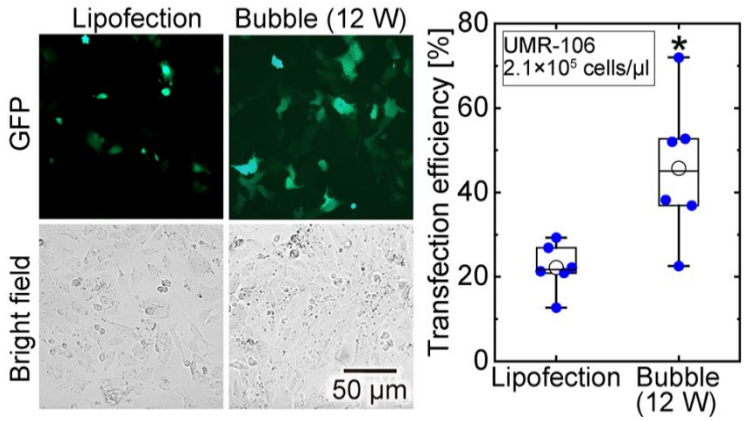

Fig. 9 Comparison of transfection efficiency of UMR-106 cells at 24 h between the electromechanical poration method and lipofectamine 3000 method. Samples were prepared without thickeners. Plasmid pEGFP-N1 was used. Bubble (12 W): bubble exposure at 12 W. Lipofection: lipofectamine 3000 treatment. *: $p < 0.05$ *vs.* samples transfected using lipofectamine. *p* values were calculated using a two-sample t-Test in OriginLab2021.

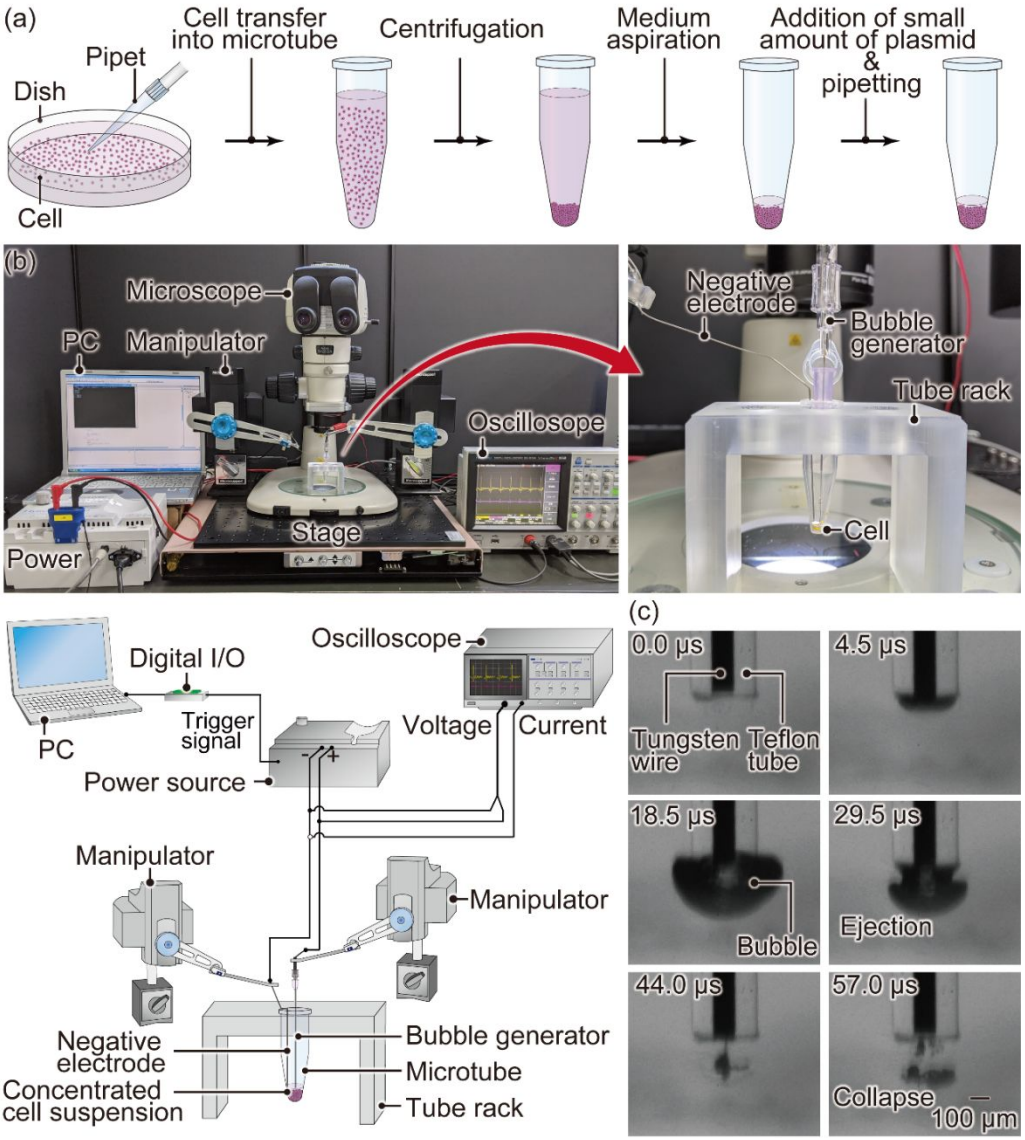

Fig. 10 Sample preparation, system configuration and device setup. (a) Sample preparation. Cells were transferred to the microtube and centrifuged to obtain a cell pellet. Then, a small amount of plasmid was added to re-suspend the cells for bubble exposure. (b) System configuration. The red arrow points to an enlarged view of the cell transfection unit. The drawing at the bottom left corner shows the detailed device configuration. (c) Bubble generation using the system.

87